REPORT DOCUMENTATION PAGE

AFRL-SR-BL-TR-02-

0145

1. AGENCY USE ONLY (Leave blank)	2. REPORT DATE	3. REPORT TYPE AND DATES COVERED
		01 Apr 98 to 31 Mar 01 FINAL

4. TITLE AND SUBTITLE
Multidimensional Multiwavelength Circuit Packet Switching using Wavelength Conversion Via four Wave mixing (FWM) in Semiconductor

5. FUNDING NUMBERS
61102F
2305/DV

6. AUTHOR(S)
Professor Blumental

7. PERFORMING ORGANIZATION NAME(S) AND ADDRESS(ES)
Univeristy of California
Cheadle Hall
Santa Barbara, CA 93106-2050

8. PERFORMING ORGANIZATION REPORT NUMBER

9. SPONSORING/MONITORING AGENCY NAME(S) AND ADDRESS(ES)
AFOSR/NE
801 North Randolph Street Rm 732
Arlington, VA 22203-1977

10. SPONSORING/MONITORING AGENCY REPORT NUMBER

F49620-98-1-0399

11. SUPPLEMENTARY NOTES

12a. DISTRIBUTION AVAILABILITY STATEMENT
APPROVAL FOR PUBLIC RELEASED; DISTRIBUTION UNLIMITED

12b. DISTRIBUTION CODE

13. ABSTRACT (Maximum 200 words)

The focus of this research project is to investigate new approaches to switching multiple wavelengths within small volumes and low power consumption that is independent of data rates We also have basic experimental results that show a path toward implementation of this type of switching component. The potential impact on future DoD and military needs will be where the movement of large amounts of data is needed in space and power sensitive applications (e.g. fighter aircraft, ship based networks, rapidly deployed networkds, harsh environments).

14. SUBJECT TERMS

20020417 260

15. NUMBER OF PAGES

16. PRICE CODE

17. SECURITY CLASSIFICATION OF REPORT	18. SECURITY CLASSIFICATION OF THIS PAGE	19. SECURITY CLASSIFICATION OF ABSTRACT	20. LIMITATION OF ABSTRACT
UNCLASSIFIED	UNCLASSIFIED	UNCLASSIFIED	UL

AFOSR Final Technical Progress Report

F49620-98-1-0399

Daniel J. Blumenthal

Department of Electrical and Computer Engineering
University of California
Santa Barbara, CA 93106
Tel: (805) 893-4168; Email: **danb@ece.ucsb.edu**

Table of Contents

1. Objective and Overview

The focus of this research project is to investigate new approaches to switching multiple wavelengths within small volumes and low power consumption that is independent of data rates. Typically, in order to switch information between multiple wavelengths, wavelength multiplexed data must first be separated using wavelength demultiplexers and multiplexers and the switching process using a separate switch for each color. This approach consumes an increased amount of space and power as more wavelengths are added and as bit rates are increased. In this project we investigate an approach that leverages a single amplifying medium to switch multiple wavelengths without requiring the components for spatial separation and number of switches that increases as then number of wavelengths goes up. Our approach employed optical nonlinearities in semiconductor optical amplifiers (SOAs) One key result of this project was results of simulation studies of multidimensional wavelength switching using quantum dot SOAs (QD-SOAs). We also have basic experimental results that show a path towards implementation of this type of switching component. Since QD-SOAs are potentially an inhomogeneously broadened gain medium, they have the potential to overcome limitations of the homogeneously broadened gain medium of bulk SOAs. The potential impact on future DoD and military needs will be where the movement of large amounts of data is needed in space and power sensitive applications (e.g. fighter aircraft, ship based networks, rapidly deployed networks, harsh environments).

2. Potential Applications

We have identified several potential applications for this technology

- WDM networks for fighter aircraft, ship communications and space/power sensitive application
- Rapidly deployed WDM networks
- Multichannel amplifiers without crosstalk
- Multiwavelength optical switches
- Multichannel wavelength converters

3. Research Topics/Issues

The following research topics and issues were covered under this project:

- Fabrication of QD-SOAs at the 1.3 micron wavelength operation region
- Modeling and simulation of optical properties of QD-SOA active region
- Optical characterization and gain measurements of QD-SOAs
- FWM in QD-SOAs
- Optical amplification in QD-SOAs

4. Motivation

Optical waveguides and optical amplifiers combined with Wavelength Division Multiplexing (WDM) enables simultaneous transmission and amplification of multiple high data-rate channels. Shown in Figure 1 is a multichannel system that employs a line amplifier to simultaneously amplify all wavelengths. This approach saves power and space by not requiring the signals to be demultiplexed, individually amplified and remultiplexed at the repeater. However, the same principal is very difficult to extend to switching.
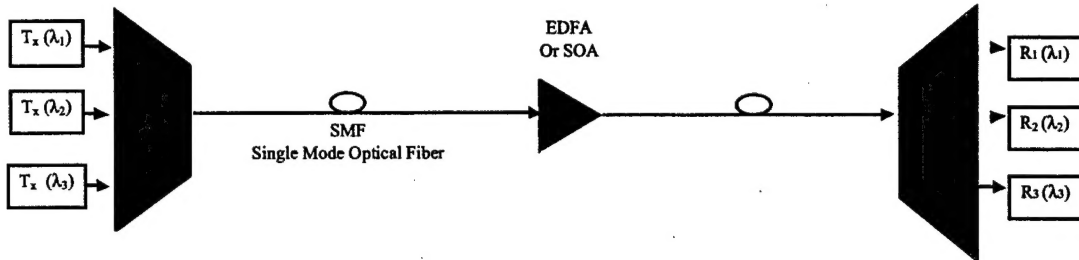

Figure 1. In-line amplification of WDM channels simultaneously using an erbium doped fiber amplifier (EDFA).

With single optical switch as shown in Figure 2, multiple WDM channels can be switched simultaneously under a single control such that all signals are direct in the same way. This is one advantage of optical switches in that the power dissipation to redirect all wavelengths using one switch is much lower than demultiplexing and using individual switches for each color. However, there are many times when it is necessary to direct each color to a different switch port using a separate control signal. In this new case, the technology does not currently exist.
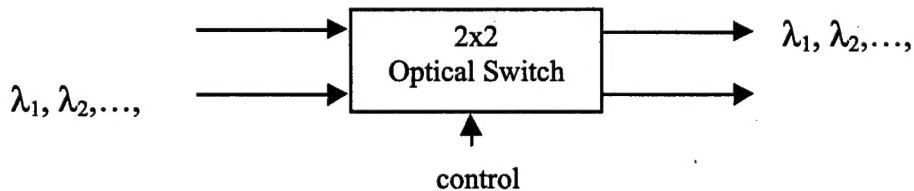

Figure 2. Switching of all wavelengths from one fiber to another using a single optical switch.

In order to switch WDM channels independently we generally use "spatial diversity" by combining wavelength multiplexing/demultiplexing with larger switches constructed out of smaller 2x2 switches as shown in Figure 3. Note that each 2x2 needs it own control signal. The power and space requirements grow as the number of wavelengths, the number of fibers and the number of switches needed to implement this approach also increase.
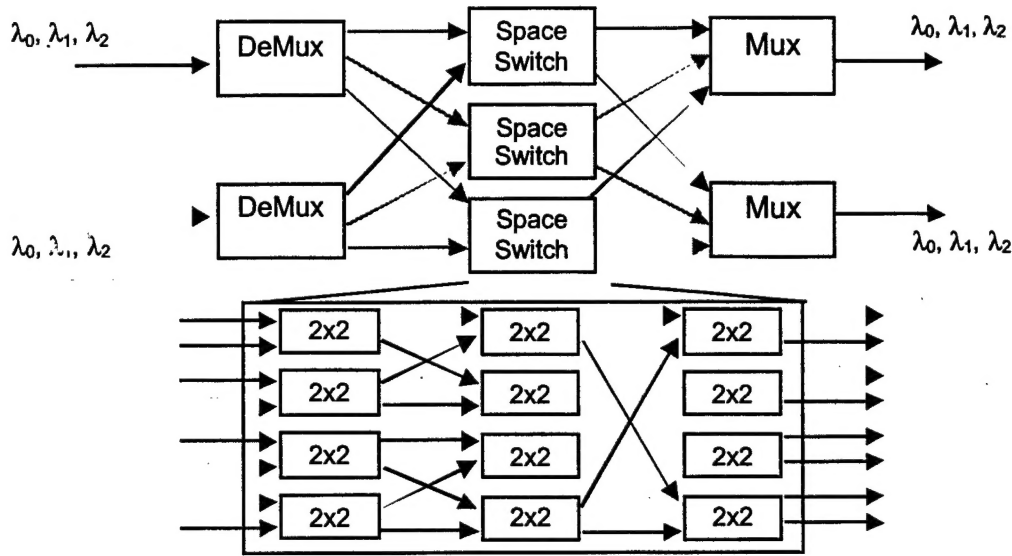
3

Figure 3. Building larger switches that can switch each wavelength separately using wavelength multiplexers, demultiplexers and multiple stages of banks of 2x2 switches.

We have proposed to use optical nonlinearities in SOAs to perform multiple switching operations within a single device [1]. This approach illustrated in Figure 4 has the potential to collapse multiple switches in the wavelength domain using WDM control signals. The use of WDM control signals also simplifies the interconnection problem to multiple switching elements, which is nontrivial for any high throughput switching technology.
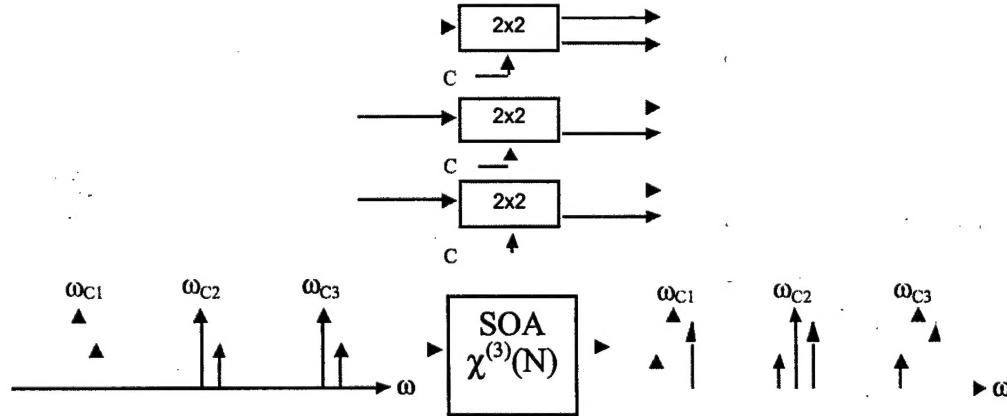

Figure 4. Collapsing multiple switches into a single switch using a spectrally segmented third order optical nonlinearity.

Trying to perform multiple FWM processes within the same bulk semiconductor (homogeneously broadend gain) is that the dynamic gratings for each pump/probe (control/signal) carrier beating will scatter light from other FWM processes creating crosstalk terms (intermods) and the intensity fluctuations of each signal will modulate the gain seen by all other signals leading to a cross-gain modulation (XGM) and cross-phase modulation (XPM) crosstalk. These crosstalk mechanisms can be summarized as:

1. Dynamic grating crosstalk: scattering of signals from a gain or phase grating generated by another pump/probe pair in the same amplifying medium.

4

2. Cross gain modulation (XGM) crosstalk: Modulation of the signal or converted signal gain due to modulation of another signal intensity located in the same amplifying medium.

In order to overcome these crosstalk limitations, and extend the number of independent FWM wavelength switches within a single SOA, we investigated the inhomogeneously broadend gain of Quantum Dot Semiconductor Optical Amplifiers (QD-SOAs) [2-5]. With this approach, each dot creates a resonance at a particular optical frequency and can be gain modulated to generate a phase/gain grating for FWM wavelength conversion. The center frequency of the gain of a quantum dot depends on the size of that dot. While materials researchers focus on trying to create uniform populations of dot sizes, here we exploit the fact that without dot size control, there is a statistical distribution of dot size, creating a distribution of gain lineshapes center frequencies that are distributed over a large bandwidth as shown schematically in Figure 5. By keeping the gain and hence the FWM isolated (in principal) to discrete spectral regions, we believe that multiple FWM wavelength conversions and hence switches can be implemented within a single device as shown in Figure 5. While in principal this is an appealing approach, there are many details and issues that must be resolved and this area became the focus of our research for this project.
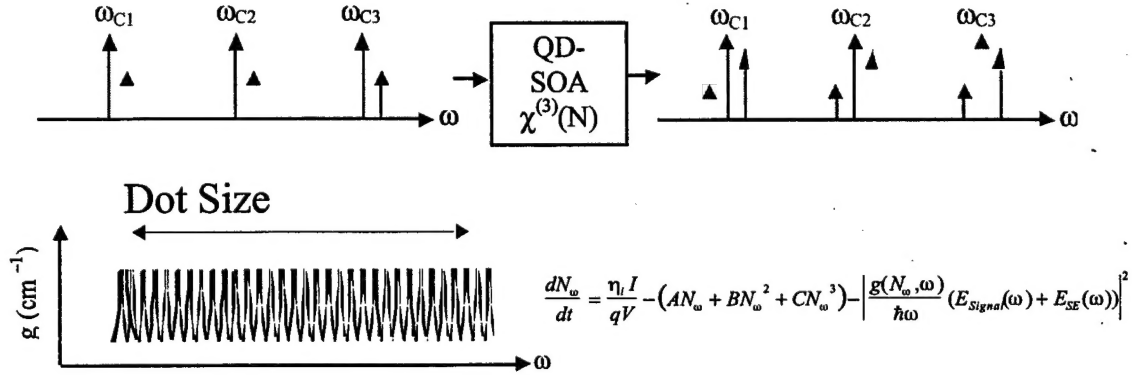

$$\frac{dN_\omega}{dt} = \frac{\eta_i I}{qV} - \left(AN_\omega + BN_\omega^2 + CN_\omega^3\right) - \left|\frac{g(N_\omega,\omega)}{\hbar\omega}\left(E_{Signal}(\omega) + E_{SE}(\omega)\right)\right|^2$$

Figure 5. FWM in a QD-SOA to realize multiple wavelength conversions/switches within a single amplifying medium.

5. Status of effort and Results

Over the course of this project we have performed several experimental demonstrations, fabricated and measured several QD-SOA samples and developed fairly sophisticated models and simulations to predict the performance and behavior of QD-SOAs. In the earlier work, using bulk active waveguides (SOAs) we demonstrated a series of results [1] including (i) single channel conversion of 12.5 Gbps pseudo-random bit sequence (PRBS) data, (ii) conversion of four 2.5 Gbps channels using a single pump and (iii) two separate conversions of 2.5 Gbps data channels using two spectrally segmented FWM process and two separate control frequencies within a single amplifier. The later demonstration represents a significant milestone in the direction of our program objectives. We advanced this phase of the demonstration to a 10 FWM conversions in a single SOA with 10 Gpbs digital channels. At this point the crosstalk degradations were too extensive to engineer the operating point of the amplifier for penalty free conversion of all channels.

With regard to the new work on FWM in QD-SOAs, to our knowledge, there has been very limited results reported on FWM in QD-SOAs. The only results that we know of so

far in the literature are D. Bimberg's group in Germany. While we have made advances in this area, we have written limited publications as we feel the work still needs to be advanced more prior to publication. To achieve the current results, we have worked closely with Rich Mirin (NIST) to fabricate and measure 1.3 micron QD-SOAs.

5.1. QD-SOA Fabrication

Long wavelength (1.31µm) single layer and double layer QD active material was grown at NIST. A schematic of the QD process is shown in Figure 6(a-c). A SEM of a region of dots shows the distribution and resulting dot gain layers are shown in Figure 6(d). We then fabricated broad stripe ridge SOA structures at UCSB and a resulting microphotograph is shown in Figure 6(e). A schematic of the QD epitaxial is shown in Figure 7.
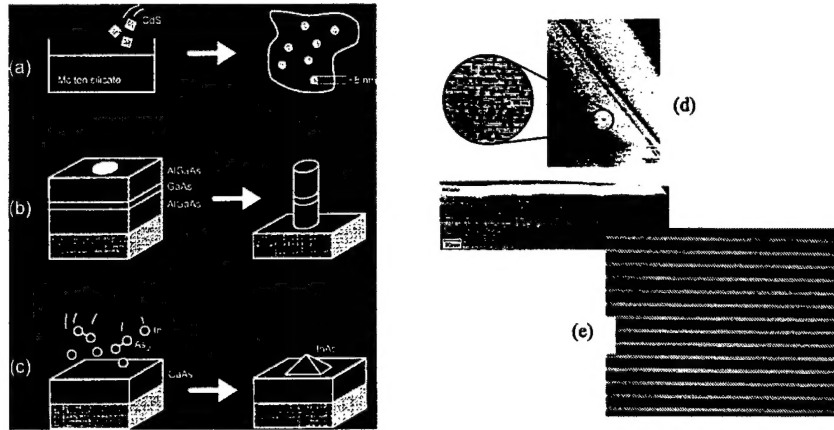

Figure 6. A schematic of the fabrication process of QD gain material (a-c), a SEM of dot distribution and active layers (d) and fabricated broad stripe QD lasers (e).

Figure 7. QD gain epitaxial material structure.

5.2. Room Temperature QD Laser Measurements

Room temperature photoluminescence measurements were made for two different epitaxial wafers. The wafers were illuminated with optical power of 4, 8, 16 (and 10 for one sample) mW. Emission peaks for sample R224 (Figure 8) shows fist excited state emission peaks at approximately 1160nm and approximately 1240nm for the ground state emission peaks. Sample B227 had emission peaks at 1220nm and 1300nm, closer to the desired wavelength. As expected we were not able to reach saturation under PL conditions.
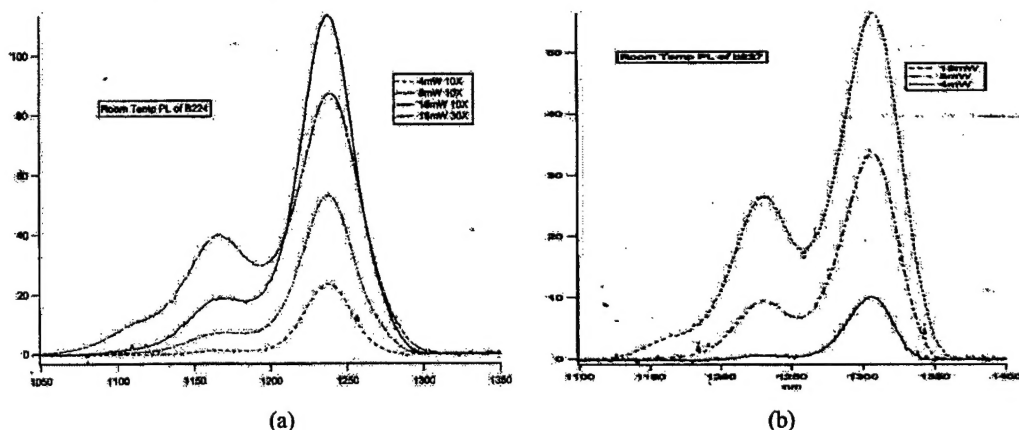

(a)   (b)

Figure 8. Room temperature photoluminescence (PL) of two QD laser samples at various illumination intensities.

Room temperature electro-luminescence (EL) measurements were made by current injection to a 2mm long broad area laser and coupling of an optical fiber to one of the output facets. Measurements were made on a real time optical spectrum analyzer as a function of injection current. The sample was maintained at a constant temperature using a current controlled peltier device (TEC). The resulting EL measurements for injection currents of 10, 20, 30, 50, 100, 150 and 200mA are shown in Figure 9.

We see in these results the expected ground excited state (1280nm) and first excited state (1210nm) emissions from the dots. The line shapes of individual dot populations are not seen at this resolution. Also, as discussed later, emission from the 2nd excited states and the wetting layer (higher energies) are not seen on this scale. By comparing the 150mA and 200mA curves it is seen that, as expected, the ground state saturates before the 1st excited state.
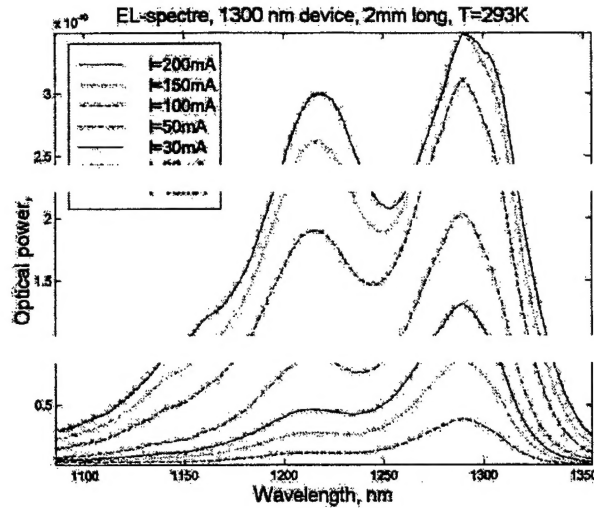
7

Figure 9. Room temperature EL measurements of a 2mm long QD broad area laser at several injection currents.

5.3. QD-SOA Model and Simulations

Given that the QD laser samples appeared to give the expected PL and EL results, we wanted to better understand the behavior and device characteristics, so a analytical model was developed and numerical simulation written. The goal of this part of the work was to develop simulation model for QD-SOAs and understand which modeling method is appropriate.

Two approaches were identified as shown in Figure 10: (i) an ordinary rate equation approach and (ii) a micro state rate equations (master equation) approach. In both cases, as shown in the center energy diagram, absorption and emission and energy transfer between any two states were accounted for.

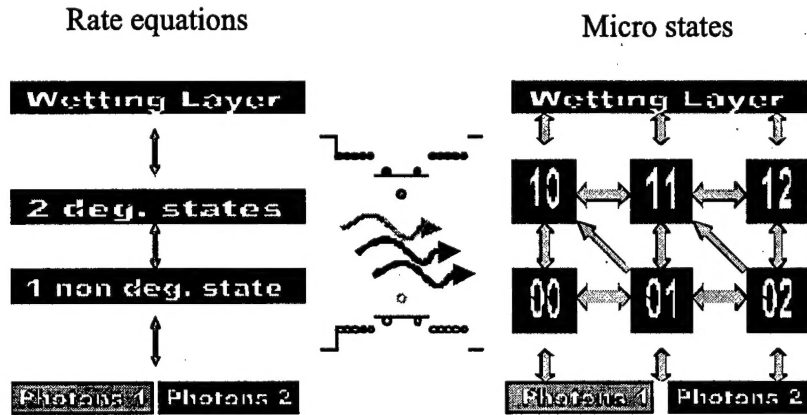Rate equations   Micro states

Figure 10. Alternate descriptions of the two level system with wetting layer, rate equations and microstates.

The rate equation model is shown schematically in more detail in Figure 11. Each dot is represented as a three level system (chosen for generality and convenience). Each pair of

8

levels are coupled by transition rates shown by the arrows where R_{cap} is the capture rate, R_e^u the escape rate, R_r^i the relaxation rate, R_e^i the excitation rate, R_{sp}^i the spontaneous emission rate and R_{sb}^i the stimulated emission/absorption rate.
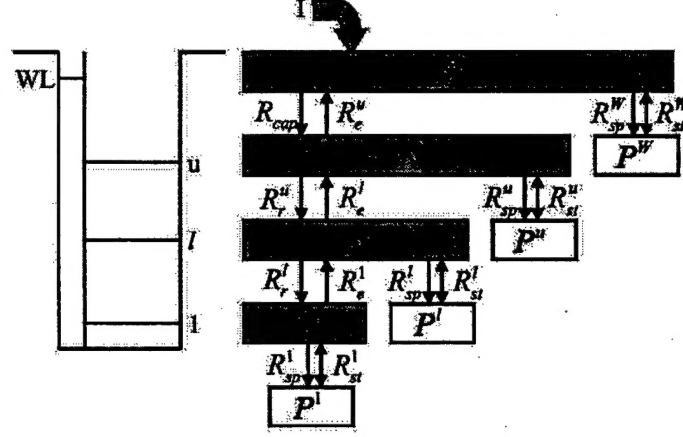

Figure 11.   Rate equation model representation for quantum dot simulation [5].

The carrier rate equations can be written [5] for carriers N^w in the wetting layer (Eqn. 1), for the carriers N^u in the upper excited state (Eqn. 2), for the carriers N^l in the lower excited state (Eqn. 3) and ground state carriers N^1 (Eqn. 4) as

(Eqn. 1) $\dfrac{dN^W}{dt} = \dfrac{I}{qV_W} + R_e^u - R_{cap} - R_{sp}^W - R_{st}^l = \dfrac{I}{qV_W} - \dfrac{N^u}{\tau_e^u}\dfrac{V_D}{V_w}f_w' - \dfrac{N^w}{\tau_{sp}^w} - \dfrac{L}{V_w}g^w\dfrac{P^w}{\hbar\omega_w}$,

(Eqn. 2) $\dfrac{dN^u}{dt} = R_{cap} + R_e^l - R_e^u - R_r^u - R_{sp}^u - R_{st}^u = \dfrac{N^w}{\tau_c}\dfrac{V_w}{V_D}f_u' + \dfrac{N^l}{\tau_e^l}f_u' - \dfrac{N^u}{\tau_e^u}f_w' - \dfrac{N^u}{\tau_0^u}f_{u-1}' - \dfrac{N^u}{\tau_{sp}^u} - \dfrac{L}{V_D}g^u\dfrac{P^u}{\hbar\omega_u}$,

(Eqn. 3) $\dfrac{dN^l}{dt} = R_r^u - R_e^1 - R_e^l - R_r^l - R_{sp}^l - R_{st}^l = \dfrac{Nu}{\tau_0^u}f_l' + \dfrac{N^1}{\tau_e^1}f_l' - \dfrac{N^l}{\tau_e^l}f_u' - \dfrac{N^l}{\tau_0^l}f_1' - \dfrac{N^l}{\tau_{sp}^l} - \dfrac{L}{V_D}g^l\dfrac{P^l}{\hbar\omega_l}$ and

(Eqn. 4) $\dfrac{dN^1}{dt} = R_r^l - R_e^1 - R_{sp}^1 - R_{st}^1 = \dfrac{N^l}{\tau_0^l}f_1' - \dfrac{N^1}{\tau_e^1}f_l' - \dfrac{N^1}{\tau_{sp}^1} - \dfrac{L}{V_D}g^1\dfrac{P^1}{\hbar\omega_1}$,

where the wetting layer (WL) volume is V_w and the total dot volume is V_D. The carrier spontaneous lifetime for the ith level is τ_{sp}^i and the optical power and photon energies interacting with carriers at the ith level are P^i and $\hbar\omega_i$. The capture and relaxation times are given by τ_c and τ_0^i and the escape and excitation times are τ_e^u and τ_e^l. The probability of finding an empty state at level i is given by $f_i' = 1 - N^i/N_{max}^i = 1 - N^i/\rho^i N_D$ and the maximum allowed carrier density at level i is given by N_{max}^i. For the wetting layer, $f_w' = 1 - f_w = 1 - \exp\left(-\dfrac{N^w H_w \pi\hbar^2}{k_B T m_e}\right)$. For optical gain in the active dot layer, from the ith level, g^l is the material gain (taken to be linearly proportional to the excess carrier density and the dot

9

confinement factor Γ_D as $g^i = \Gamma_D a_i (2N^i - N^i_{max})$. For optical gain in the wetting layer, a similar equation gives the gain as $g^w = \Gamma_w a_w (N^w - N_w)$.

The gain in a QD SOA for a photon population generated at level i can be approximated by (Eqn. 5) assuming the gain is uniform over the length of the amplifier (L) and the fraction of spontaneous emission that couples into the forward propagating mode is given by β_{spont}.

(Eqn. 5) $\qquad P^i(L) = P^i(0)\exp(g^i_{net}L) + \beta_{spont}\dfrac{N^i V_D}{\tau^i_{sp} L}\hbar\omega_i \dfrac{\exp(g^i_{net}L)-1}{g^i_{net}}$

The Master Equation Model utilizes the dot states instead of carrier states as in the rate equation model. The QD is assumed to be in an isolated system that supports a specific set of quantum mechanical eigenstates. The state of the dot is modified by interaction with the surroundings, which if assumed to be infinite are unperturbed with respect to changes in the dot state. The probability that the dot is in state |d> is defined as x_d and the time varying change for this probability is governed by (Eqn. 6) [3,5]

(Eqn. 6) $\qquad \dfrac{\partial x_d}{\partial t} = \displaystyle\sum_{i=1}^{n_d} x_i(t)R^{i,d}_{tot} - x_d(t)R^{d,i}_{tot}$

where the total transition rate from dot state |d> to |i> is given by $R^{d,i}_{tot}$ and the total number of possible states is n_d.

The example QD system within the dotted box shown in Figure 12 has 6 states with |1> at the lowest energy and |6> at the highest energy. The state of the dot is modified by interaction with the wetting layer and the photonic populations. The rate of transition between any two states is shown as is the probability of the dot being in a certain state. In order to facilitate computation, the following assumptions were made:

- Carrier capture is considered into the upper level only

- Carrier relaxation and excitation to the nearest neighboring level only is allowed

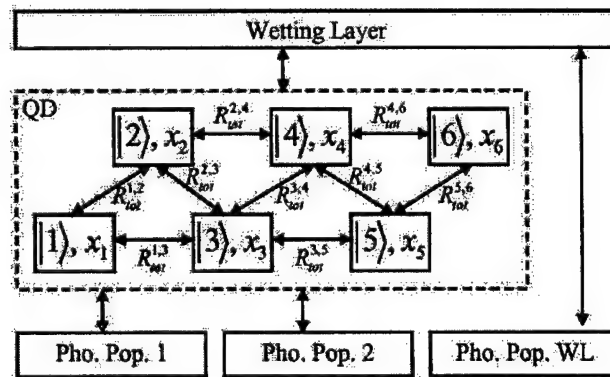- No dot state transitions involving two simultaneous carrier transitions take place

Figure 12.   Master equation model of quantum dot transitions [5].

The master equations describe the time varying change in probability of state transition and the time varying change in wetting layer carrier density as described in terms of rates (Eqn. 7) and in more detail (Eqn. 8).

$$\frac{\partial x_d}{\partial t} = \sum_{i=1}^{n_c}\sum_{l=1}^{u}\left(R_{e,l}^{i,d} + R_{r,l}^{i,d} + R_{cap}^{i,d} + R_{absl}^{i,d} + R_{st,l}^{i,d} + R_{sp,l}^{i,d}\right)x_i$$

(Eqn. 7)

$$-\sum_{i=1}^{n_c}\sum_{l=1}^{u}\left(R_{e,l}^{i,d} + R_{r,l}^{i,d} + R_{cap}^{i,d} + R_{abs,i}^{i,d} + R_{st,l}^{i,d} + R_{sp,l}^{i,d}\right)x_d$$

$$\frac{\partial x_d}{\partial t} = \sum_{i=1}^{n_c}\left(\frac{f_w'}{\tau_c^u} + \frac{N^w}{\tau_c N_D}\frac{V_w}{V_D}\frac{U_{i,d}^u}{\rho_{-s}^u}\right)x_i - \left(\frac{f_w'}{\tau_e^u} + \frac{N^w}{\tau_c N_D}\frac{V_w}{V_D}\frac{U_{i,d}^u}{\rho_{-s}^u}\right)x_d$$

$$+ \sum_{i=1}^{u}\left(\frac{X_{i,d}^l}{\tau_c^u} + \frac{1}{\tau_e^l} + \frac{a_l}{\sigma}P^l U_{i,d}^l + D_{i,d}^l\left(\frac{a_l}{\sigma}P^l + \frac{1}{\tau_{sp}^l}\right)\right)x_i$$

(Eqn. 8)

$$- \left(\frac{X_{d,i}^l}{\tau_0^l} + \frac{1}{\tau_e^l} + \frac{a_l}{\sigma}P^l U_{d,i}^l + D_{d,i}^l\left(\frac{a_l}{\sigma}P^l + \frac{1}{\tau_{sp}^l}\right)\right)x_d$$

where $U_{d,i}^l$ is the "up transition strength" that describes the increase in carriers at level l by one and $D_{d,i}^l$ is the "down transition strength" that describes the decrease in carriers at level l by one. The equation governing the wetting layer carrier density is given by (Eqn. 9).

$$\frac{\partial N^w}{\partial t} = \frac{I}{qV_w} - \frac{N^w}{\tau_w} - \frac{L}{V_w}g^w P^w + \frac{V_D}{V_w}N_D\sum_{d,i}^{n_c}\left(R_{e,u}^{d,i} - R_{cap}^{d,i}\right)x_d$$

(Eqn. 9)

$$= \frac{I}{qV_w} - \frac{N^w}{\tau_w} - \frac{L}{V_w}g^w P^w + \sum_{d,i}^{n_d}\left(N_D\frac{V_D}{V_w}\frac{D_{d,i}^u}{\tau_e^u}f_w' - \frac{N^w}{\tau_c}\frac{U_{d,i}^u}{\rho_{-s}^u}\right)$$

The optical mode gain factor is found by summing all stimulated emission rates from a state and subtracting all absorption rates from that state. The result is given in (Eqn. 10)

(Eqn. 10) $\quad g^l = a_l\Gamma_D N_D\sum_{d,i}^{n_d}\left(D_{d,i}^l - U_{d,i}^l\right)x_d P^l = a_l\Gamma_D\left(2N^l - N_{max}^l\right)P^l$

The time varying change in photon density can be derived from combining the photon population growth for a propagating mode in the amplifier

(Eqn. 11) $\quad \frac{\partial P^l}{\partial t} = \left(g^l - \alpha_{in}^l\right)P^l + \beta_{spont}\frac{V_D}{L}\hbar\omega_l\frac{N^l}{\tau_{sp}^l}$

An example steady state calculation of the carrier density for the ground and excited state levels in the dots and wetting layer is shown in Figure 13. As seen in the experimental measurements, the ground state carrier density increase linearly for low injection current levels and starts to saturate as the excited state levels start to be populated. When the excited states saturate, the wetting layer starts to fill with carriers and increase linearly. These results do not include the effects of amplified spontaneous emission (ASE).
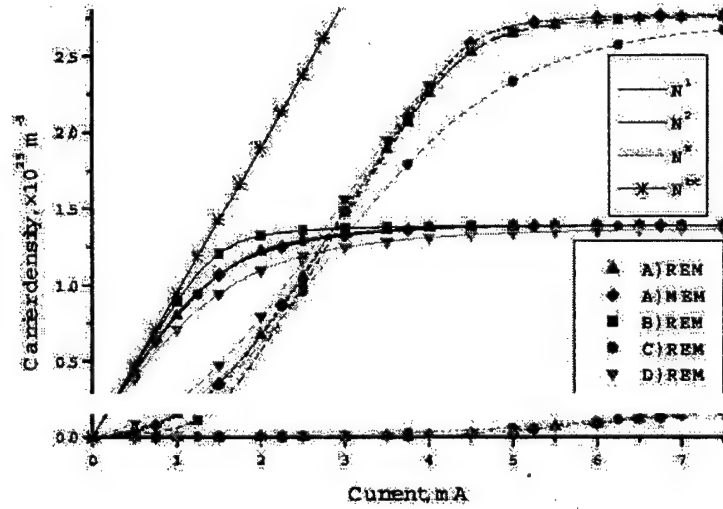
11

Figure 13. Steady state carrier density for quantum dots and wetting layer [5].

Dynamic modeling of the states can illustrate how the states fill, saturate and where lasing occurs as the device is turned on and off. Figure 14 illlustrates how the 6 states in the previous example fill and saturate with time. An interesting prediction is that of momentary lasing of certain states, an effect that has not been experimentally verified in this project.
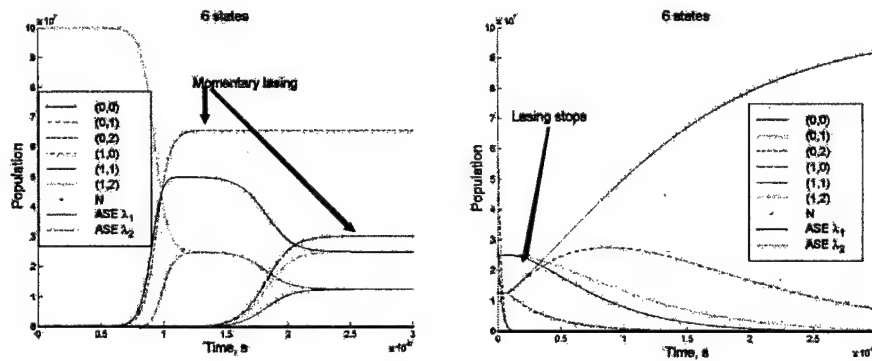

Figure 14. Simulation of carrier dynamics.

The effects of saturation predicted by the equations an described in the first part of this report, are shown in more detail in Figure 15.
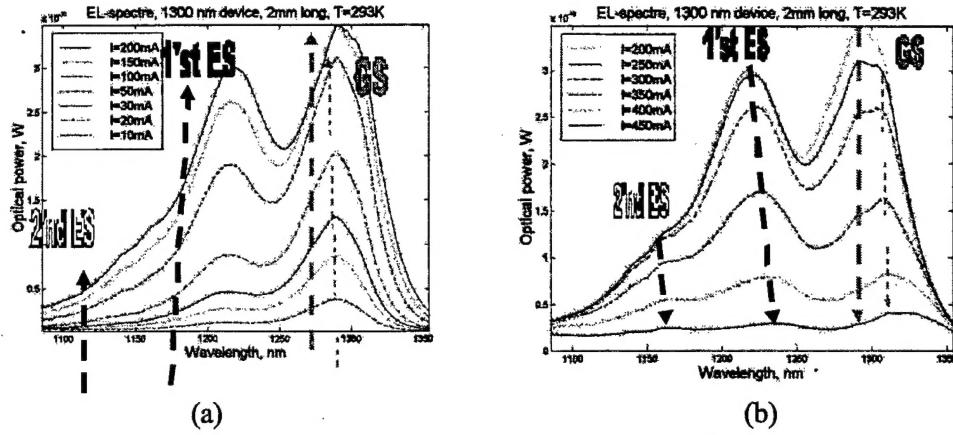
Figure 15. Experimental verification of steady state carrier densities by observing optical output spectra.

We also used this model to simulate the spontaneous emission and the power vs. current curves (P-I) as shown in Figure 16a and experimentally confirmed Figure 16b.
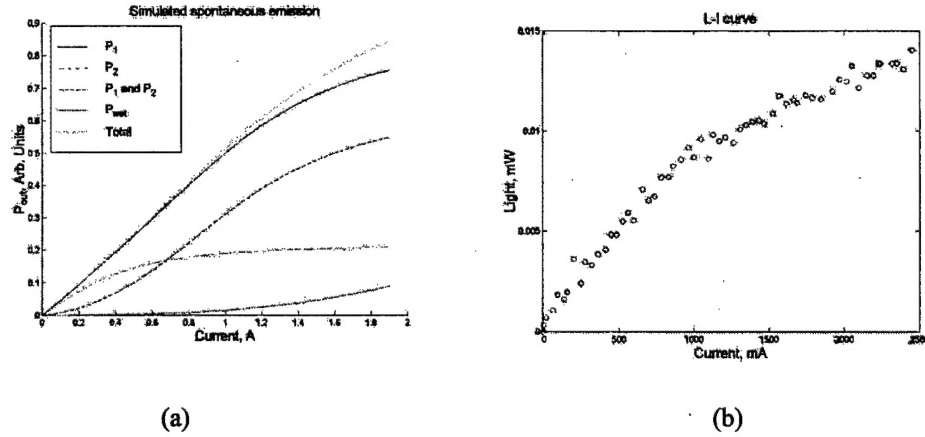

(a)   (b)

Figure 16. Quantum dot semiconductor optical amplifier (a) spontaneous emission simulation and (b) experimental measurement.

6. Accomplishments/New Findings:

We have demonstrated that simultaneous, independently controlled wavelength conversion of two digital channels is possible using four-wave mixing in a single semiconductor optical amplifier. This result is significant in the field of wavelength conversion and switching using nonlinearities in SOAs as it demonstrates that information may be spectrally segmented and processed/switched independently in a single device. This result is one of the intended objectives for our original proposal and allows complex information processing and switching systems to be folded into highly functional devices. The FWM wavelength switching operation is independent of bit-rate and formats and allows upgrade of data path without additional energy expenditures.

We have also demonstrated results on fabrication, testing and modeling/simulation of quantum dot semiconductor amplifiers that show promise to realize an inhomogeneously

13

broadend gain medium that can be used to scale the switching architecture addressed above. The results of this work includes a new state modeling approach to QD-SOAs that can describe the steady state and dynamic behavior of these amplifiers.

A summary of the potential advantages of QD-SOAs is summarized in Table 1. The issues that remain to be addressed next include

- Fabrication of QD-SOAs with large optical overlap factor (greater than 10 layer of dots most likely needed).

- Fabrication of QD-SOAs with large enough optical gain to demonstrate positive fiber to fiber gain

- Demonstration of multiwavelength FWM using QD-SOA

- Demonstration of multichannel amplification using QD-SOA

- Further verification of state model

- Pump-probe dynamic gain measurements at both lower temperature and room temperature

These results have the potential application to Air Force mission in terms of high performance communications and computing technologies. The potential Air Force and civilian technology applications include switching fabrics for low temperature supercomputers, distributed switching systems for computing and telecommunications, and high performance information processing elements for ultra high throughput data reduction.

Table 1. Advantages of QD-SOAs

High g_{mat}	10^5 cm^{-1} in QD vs. $5*10^3$ cm^{-1} in QW
High differential gain $\Rightarrow$ Low α value	$2*10^{-12}$ cm^2 QD/ $5*10^{-16}$cm^2 ^{QW} $\Rightarrow$ 0-1 QD/ 1-2 QW
Low threshold current	1-10 mA/cm^2
High Γ_0	425 K varies with temp.
High injection efficiency	
Low coupling between populations	
Low out-of-band ASE (in principle)	

7. Future Work

- Develop high gain long wavelength SOAs

- Demonstrate net gain QD-SOAs

- Demonstrate multichannel amplification and measure XGM crosstalk

- Perform FWM wavelength conversion and measurements

- Perform low temperature EL measurements

14

8. Personnel Supported:

Graduate Students:

Christoph Scholz

Milan Masonovic

Tommy Berg (TUD)

PostDoctoral Fellows:

Bengt-Erik Olsson

Faculty

Daniel J. Blumenthal

9. Publications:

[1] C. J. Scholz, L. Dubertrand and D. J. Blumenthal. Two Independently Controlled Wavelength Conversions Using Four-Wave Mixing in a Single Semiconductor Optical Amplifier. Submitted for publication in *IEEE Photonics Technology Letters,* 1997.

[2] R. Mirin, D. J. Blumenthal, "Quantum Dot Semiconductor Optical Amplifiers," *OSA Topical Meeting on Advanced Semiconductor Lasers and Their Applications '99 (ASLA '99),* Paper AthD4-1, pp. 153-155, Santa Barbara, CA, July 21-23 (1999).

[3] T. Berg, D. J. Blumenthal and J. Mork, "Modeling quantum dot semiconductor optical amplifiers," Technical Report, University of California, Santa Barbara, CA, 2000.

[4] "Quantum Dot Semiconductor Optical Amplifiers," R. P. Mirin, D. J. Blumenthal, <u>Trends in Optics and Photonics Series: Volume 32, Advanced Semiconductor Lasers and Their Applications,</u> pp. 183-185, Eds. Leo Holberg and Robert Lang, (2000).

[5] T. Berg, "Modeling of Quantum-Dot Amplifiers," Masters Thesis, Technical University of Denmark, 2001.

10. Interactions/Transitions:

- Richard Mirin, NIST: Rich designed and fabricate 1.0 micron stripe quantum dot lasers in the first phase and grew 2 layer dot material for the second phase.

- Evelyn Hu, UCSB: Has been part of active planning to look at quantum dot photonic bandgap structures as a potential future direction for this work.

- Technical Program CommitteeHot Interconnects VIII2001

- General Chair OSA Topical Meeting on Photonics in Switching   2001

- Technical Program CommitteeOpticom 2000

- General Chair Optical Summit   2000

- Guest Speaker Cisco University Research Program   2000

- Program Committee Chair   OSA Top. Mtng. on Photonics in Switching 1999

- Program Committee Chair   Optical Internetworking Conference   1999

- Program Committee Member Conference on Optical Fiber Communications (OFC) 1997-2000

- Workshop Organizer OFC Workshop on Optical Signal Processing For Optical Networks   2000

- Program Committee Member Conference on Lasers and Electrooptics (CLEO) 1999-2001

11. New discoveries, inventions, or patent disclosures.

None

12. Honors/Awards:

- Presidential Early Career Award for Scientists and Engineers (PECASE) White House/DOD   1999

- Best Transactions Paper Award   IEEE Education Society   1999

- Young Investigator Program (YIP)Office of Naval Research   1997

- Senior Member   IEEE   1997

- National Young Investigator (NYI) National Science Foundation 1994

13. Editing Journals

- Associate Editor   SPIE Optical Networks Magazine   2001 - Present

- Associate Editor   IEEE Photonics Technology Letters   1997 to 2000

- Associate Editor   IEEE Transactions on Communications   1996 to 1999

- Guest Editor   IEEE Journal of Lightwave Technology Special Issue on Photonic Packet Switching   December 1998